11-1-2018

Information-Driven Inverse Approach to Disordered Solids: Applications to Amorphous Silicon

Dil K. Limbu
University of Southern Mississippi

Raymond Atta-Fynn
University of Texas at Arlington, attafynn@uta.edu

David A. Drabold
Ohio University, drabold@ohio.edu

Stephen R. Elliott
University of Cambridge

Parthapratim Biswas
University of Southern Mississippi, partha.biswas@usm.edu

Information-driven inverse approach to disordered solids: Applications to amorphous silicon

Dil K. Limbu,[1,*] Raymond Atta-Fynn,[2,†] David A. Drabold,[3,‡] Stephen R. Elliott,[4,§] and Parthapratim Biswas[1,‖]

[1]*Department of Physics and Astronomy, The University of Southern Mississippi, Hattiesburg, Mississippi 39406, USA*

[2]*Department of Physics, University of Texas, Arlington, Texas 76019, USA*

[3]*Department of Physics and Astronomy, Ohio University, Athens, Ohio 45701, USA*

[4]*Department of Chemistry, University of Cambridge, Cambridge CB2 1EW, United Kingdom*

(Received 24 August 2018; published 8 November 2018)

Diffraction data play an important role in the structural characterizations of solids. While reverse Monte Carlo (RMC) and similar methods provide an elegant approach to (re)construct a three-dimensional model of noncrystalline solids, a satisfactory solution to the RMC problem is still not available. Following our earlier efforts, we present here an accurate structural solution of the inverse problem by developing an information-driven inverse approach (INDIA). The efficacy of the approach is illustrated by choosing amorphous silicon as an example, which is particularly difficult to model using total-energy-based relaxation methods. We demonstrate that, by introducing a subspace optimization technique that sequentially optimizes two objective functions (involving experimental diffraction data, a total-energy functional, and a few geometric constraints), it is possible to produce models of amorphous silicon with very little or no coordination defects and a pristine gap around the Fermi level in the electronic spectrum. The structural, electronic, and vibrational properties of the resulting INDIA models are shown to be fully compliant with experimental data from x-ray diffraction, Raman spectroscopy, differential scanning calorimetry, and inelastic neutron scattering measurements. A direct comparison of the models with those obtained from the Wooten-Winer-Weaire approach and from recent high-quality molecular-dynamics simulations is also presented.

DOI: 10.1103/PhysRevMaterials.2.115602

I. INTRODUCTION

The reconstruction of three-dimensional models of complex noncrystalline solids from experimental data constitutes an archetypal example of inverse problems in materials modeling. Inverse approaches provide a distinct route to design complex disordered materials by directly incorporating a set of experimental observables in simulation methodologies. The resulting atomistic models thus exhibit a high degree of compliance with a set of experimental data, and the method, by construction, eliminates the need for accurate total-energy functionals, which are necessary for conventional simulations. A classic example is the reverse Monte Carlo (RMC) method [1–5], which attempts to construct a three-dimensional model of disordered solids by inverting experimental diffraction data in conjunction with a few structural constraints. However, the difficulty associated with inverting one-dimensional pair-correlation diffraction data in the presence of competing structural constraints, which leads to a difficult nonconvex optimization problem, has been a major obstacle in producing realistic structural solutions from RMC simulations. Although the method has been employed for a variety of disordered solids [3], the problem is particularly acute for highly coordinated systems, such as amorphous silicon (*a*-Si) and tetrahedral amorphous carbon (*ta*-C). To our knowledge, none of the RMC-derived models of *a*-Si reported in the literature [1–5] to date show a pristine gap in the electronic density of states around the Fermi level and a low defect density as observed in electron spin resonance (ESR) experiments [6].

Inverse problems are often characterized by their ill-conditioned nature and they are notoriously difficult to solve satisfactorily [7]. In the context of materials modeling, the difficulty primarily arises from the volume of structural (and additional) information to be incorporated in the problem by constructing suitable penalty/constraint functions and the subsequent optimization of an objective function (involving experimental data and constraint functions) in a high-dimensional solution space. The presence of hierarchy among higher-order correlation functions [8,9] suggests that a minimal number of constraints and experimental data sets need to be included in the problem in order to produce structurally unique models. However, the inclusion of too much information can make very difficult the resulting nonconvex optimization problem and its accurate solution that satisfies the requirements of a physical model.

An approximate solution of the constrained RMC problem for *a*-Si was proposed by some of us more than a decade ago [1]. While this approach produced correctly the two- and three-body atomic correlation functions, as well as a reasonably good electronic density of states (EDOS) with a hint of a spectral gap in the vicinity of the Fermi level, the presence of a significant number of coordination defects (e.g., threefold- and fivefold-coordinated atoms) limits the

*dil.limbu@usm.edu
†attafynn@uta.edu
‡drabold@ohio.edu
§sre1@cam.ac.uk
‖Corresponding author: partha.biswas@usm.edu

applicability of the method and the resulting models for high-quality predictive studies of amorphous silicon. Although a number of hybrid or related methods [10–16], i.e., methods that involve a total-energy functional in RMC simulations in addition to scattering data, have been developed in the last decade to produce improved structural models of *a*-Si, none of the methods lead to atomistic models that can match the high quality of the bond-switching Wooten-Winer-Weaire (WWW) models [17–19]. The purpose of this paper is to present an information-driven inverse approach (INDIA), combining experimental data and constraint information with a total-energy functional to yield high-quality atomistic models of amorphous silicon. We demonstrate that the resulting structural models produce a clean gap in the electronic spectrum around the Fermi level with a few coordination defects. The atomistic models from this approach represent the very best of its class and they are comparable to those obtained from the WWW method.

In recent years, information-based approaches have played a crucial role in designing complex materials [10–13,16,20–22]. Molecular dynamics (MD) simulations, using knowledge-based interactions obtained via machine-learning algorithms, have been employed to produce high-quality MD models of *a*-Si [23]. Likewise, experimental data from nuclear magnetic resonance and infrared spectroscopy have been employed profitably to understand the microstructure of hydrogen in *a*-Si:H and the distribution of extended inhomogeneities (e.g., voids) in *a*-Si [24–27]. Electronic information too, from electronic densities of states, has been used in an effort to control and engineer the band gap of *a*-Si using constrained molecular-dynamics simulations [28]. Thus, the incorporation of relevant structural [1], electronic [28], NMR [26], and IR [29] information played a decisive role in simulations, not only to develop better structural models but also to understand physical properties of the amorphous state that were not accessible from using conventional atomistic simulations. This observation also applies to the WWW method. An examination of the latter suggests that the so-called WWW bond switches essentially introduce five-member and seven-member rings in crystalline or disordered silicon networks while maintaining fourfold coordination for each atom, coupled with the minimization of the Keating potential energy to obtain local minima on the potential-energy surface (PES). Thus, the application of bond switches in the WWW method can be viewed as an inclusion of topological information (i.e., five- and seven-member rings) in simulations that greatly facilitates the system to explore the relevant region of the PES consistent with the induced ring topology and fourfold coordination and to determine amorphous configurations of silicon in the resulting procedure.

The remainder of the paper is as follows. In Sec. II, we present an information-driven inverse approach (INDIA) that entails optimization of an augmented objective function, incorporating experimental diffraction data, a few structural constraints, and a total-energy functional. We show that the difficulty associated with the optimization of the augmented objective function can be considerably reduced by introducing a subspace optimization technique, which sequentially optimizes total-energy and experimental diffraction data (including a few geometrical constraints) in a self-consistent manner to determine optimal structural solutions, satisfying experiments and a total-energy functional simultaneously. Section III discusses the results from the simulations by examining structural, electronic, and vibrational properties of the resultant *a*-Si models. A comparison of the results with experimental data and those from the WWW and high-quality molecular-dynamics models [23,30] of identical size from the literature are also presented here. The conclusions of this work are presented in Sec. IV.

II. COMPUTATIONAL METHOD

In conventional RMC simulations, one attempts to invert a set of experimental diffraction data $F_{\rm ex}(k)$ by writing an objective function [3–5]

$$\chi^2(\mathbf{R}) = \sum_i \left[\frac{F_{\rm ex}(k_i) - F_c(k_i;\mathbf{R})}{\sigma(k_i)}\right]^2 + \sum_l \lambda_l\, C_l(\mathbf{R}), \quad (1)$$

where $F_c(k;\mathbf{R})$ correspond to simulated diffraction data obtained from a three-dimensional distribution of atoms $\mathbf{R}$, $\sigma(k_i)$ is the error associated with $F_{\rm ex}(k_i)$, and C_l are a number of structural constraints, providing additional information on the atomistic properties of the solid. The coefficients λ_l are weights associated with C_l, which determine the relative strength of the constraints in simulations. While Eq. (1) appears to present a well-posed inverse problem [31,32] for structural determination of a solid, a direct determination of an *accurate* optimal physical solution of the resulting nonconvex optimization problem has proven to be too difficult to obtain, owing to the high dimensionality of the search space and the presence of competing constraints in Eq. (1). The information-driven strategy adopted here relies on the following two observations: (a) an optimal structural solution should originate from the region of the solution space that simultaneously satisfies a set of experimental data and a total-energy functional; (b) the solution must represent a good local minimum on the potential-energy surface and that it ought to be consistent with the structural constraints included in Eq. (1) (see Fig. 1). Toward this end, we form an augmented objective function $\mathcal{P}(E,\mathbf{R})$, which is the direct product of a total-energy functional $E(\mathbf{R})$ and the function χ^2 in Eq. (1),

$$\begin{aligned}
\mathcal{P} &\equiv E(\mathbf{R}) \otimes \chi^2(\mathbf{R}) \\
&\equiv E(\mathbf{R}) \otimes \left[\sum_i \left(\frac{F_{\rm ex}(k_i) - F_c(k_i;\mathbf{R})}{\sigma(k_i)}\right)^2 + \sum_l \lambda_l C_l(\mathbf{R})\right] \\
&\equiv \left[E(\mathbf{R}) \otimes \sum_i \left(\frac{F_{\rm ex}(k_i) - F_c(k_i;\mathbf{R})}{\sigma(k_i)}\right)^2\right] \\
&\quad \oplus \left[E(\mathbf{R}) \otimes \sum_l \lambda_l C_l(\mathbf{R})\right] \\
&\equiv \chi^2_M \oplus \chi^2_K. \qquad (2)
\end{aligned}$$

In Eq. (2), χ_M is the objective function in subspace $\mathcal{M}$, spanned by the total-energy functional and experimental diffraction data. A similar definition applies to χ_K in subspace $\mathcal{K}$, where experimental diffraction data are replaced by a set

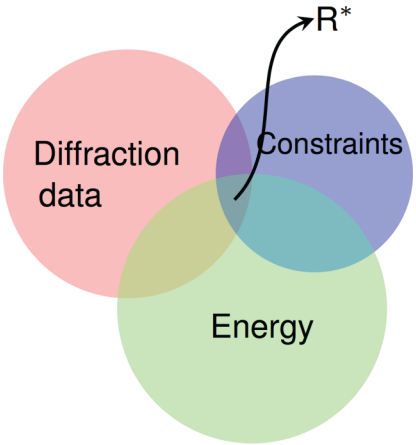

FIG. 1. A schematic illustration of the augmented space $\mathcal{P}$, consisting of the objective-function spaces spanned by the experimental data (red), constraint information (blue), and a total-energy functional (green). An optimal structural solution $\mathbf{R}^*$ corresponds to the region of intersection of the three circles.

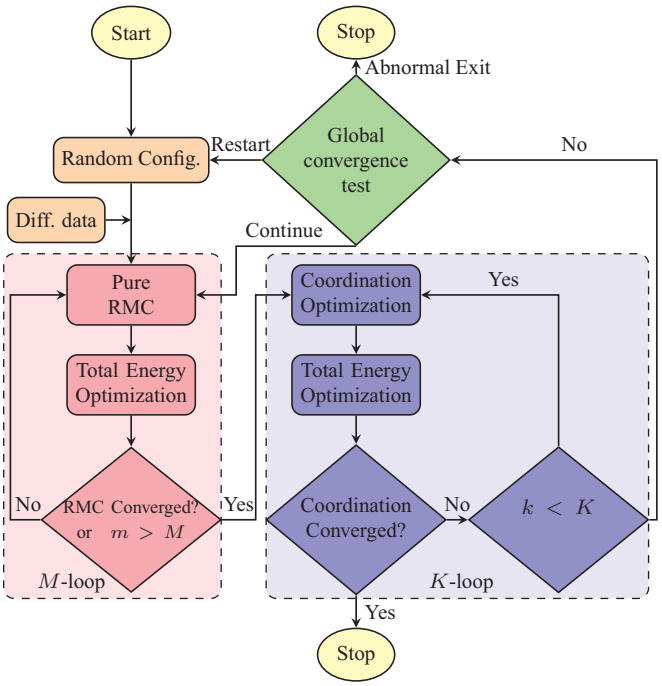

FIG. 2. A flowchart showing information flow during simulations. The subspace coupling between the M loop and K loop reduces the computational complexity of the optimization problem and leads to the generation of nearly defect-free configurations of amorphous silicon.

of structural constraints [33]. The symbols $\otimes$ and $\oplus$ stand for the operation of direct product and direct sum between the subspaces that form the augmented objective function space $\mathcal{P}$. A schematic illustration of these regions and their relationship to $\mathcal{P}$ is shown in Fig. 1. All optimal structural solutions correspond to the region of intersection between the subspaces via the mapping $f : \mathbf{R} \rightarrow \mathcal{P}$. We emphasize that, while several optimal solutions might exist that can differ from each other microscopically, it is necessary that they are macroscopically similar in order to be considered as correct physical solutions of the problem. In the following, we provide an ansatz to obtain optimal structural solutions $\mathbf{R}^*$ that simultaneously satisfy the objective functions χ_M and χ_K in subspaces $\mathcal{M}$ and $\mathcal{K}$, respectively. The procedure for determining an optimal solution in $\mathbf{R}$, by jointly optimizing χ_M and χ_K, consists of the following steps.

(1) Start with a random distribution of atoms and optimize the objective function χ_M to fit experimental diffraction data and a total-energy functional in $\mathcal{M}$. This is achieved by conducting a reverse Monte Carlo simulation to fit the diffraction data and minimizing the total potential energy via the conjugate-gradient (CG) or an appropriate method in a self-consistent manner. We refer to this step as the M loop (see Fig. 2). The convergence of this self-consistent loop is obtained by specifying a maximum value of M and tolerance values for RMC fitting and total-energy relaxations;

(2) The structural solution $\mathbf{R}^*_M$, obtained on successful completion of step 1, is subjected to further treatment so that the objective function χ_K, involving a coordination constraint [34] $C_l(\mathbf{R})$, and a total-energy functional $E(\mathbf{R})$, is now optimized. The optimization is performed as before for fitting a coordinate-constraint function using a second RMC simulation and total-energy optimization via CG relaxations or a suitable scheme. The step is indicated as the K loop in Fig. 2 and the convergence is handled in a similar manner by specifying tolerance values for atomic coordination and total energy.

(3) To ensure that the final solution satisfies both the objective functions χ_M and χ_K, a coupling is established between $\mathcal{M}$ and $\mathcal{K}$ so that the resulting output $\mathbf{R}^*_K$, from step 2, can be fed back to the M loop to achieve self-consistency between $\mathbf{R}^*_M$ and $\mathbf{R}^*_K$, using suitable convergence criteria. The latter involves specification of a coordination-defect density, a root-mean-square deviation of the bond-angle distribution, and a goodness-of-fit of the diffraction data in RMC simulations within the feedback loop (via a green diamond), which determine the final converged solution $\mathbf{R}^*$. In the event that a converged solution cannot be obtained for a given number of iterations, the program can either continue by generating a new random configuration or exit the loop prematurely with the current solution.

A flowchart of the optimization program is shown in Fig. 2. The subspace optimizations of χ_M and χ_K are indicated in the flowchart as shaded regions in light red and light blue colors, respectively. The two regions are connected by a feedback loop through a green diamond in Fig. 2 in order to achieve a self-consistent solution in subspaces χ_M and χ_K.

For total-energy optimizations, one can choose an appropriate classical, semiclassical, or quantum-mechanical force field, depending upon the complexity of the problem to be addressed. Here, we have employed the modified Stillinger-Weber (SW) potential [35,36]

$$E(\mathbf{R}) = \frac{1}{2}\sum_{i=1}^{N}\sum_{\substack{j=1\\(j\neq i)}}^{N} v_2(r_{ij}) + \sum_{i=1}^{N}\sum_{\substack{j=1\\(j\neq i)}}^{N}\sum_{\substack{k=1\\(k\neq i)\\(k>j)}}^{N} v_3(\boldsymbol{r}_{ij}, \boldsymbol{r}_{ik}), \qquad (3)$$

where v_2 and v_3 are the two-body and three-body contributions to the total potential energy, respectively, and they are

TABLE I. Modified Stillinger-Weber potential parameters [35].

ϵ (eV)	λ	σ (Å)	γ	A	B	a	p
1.648 33	31.5	2.0951	1.20	7.049 556 277	0.602 224 558 4	1.80	4

given by

$$v_2 = \begin{cases} \epsilon A\left[B\left(\frac{r_{ij}}{\sigma}\right)^{-p} - 1\right] e^{\left(\frac{\sigma}{r_{ij}-a\sigma}\right)}, & \text{if } r_{ij} < a\sigma \\ 0, & \text{otherwise} \end{cases}$$

and

$$v_3 = \begin{cases} \epsilon\lambda\left(\cos\theta_{jik} + \frac{1}{3}\right)^2 e^{\left(\frac{\sigma\gamma}{r_{ij}-a\sigma} + \frac{\sigma\gamma}{r_{ik}-a\sigma}\right)}, & \text{if } r_{ij}, r_{ik} < a\sigma \\ 0, & \text{otherwise.} \end{cases}$$

In Eq. (3), r_{ij} is the distance between two atoms at sites i and j, and θ_{jik} is the angle subtended at site i by the vectors $\mathbf{r}_{ij}$ and $\mathbf{r}_{ik}$. We employed the modified SW potential parameters from Ref. [35], which are listed in Table I. Throughout the work, we have used the experimental density of a-Si of 2.25 g/cm^3 and a maximum value of $M = 200$ and $K = 1000$ for achieving self-consistency within the M loop and K loop, respectively. To compute the electronic and vibrational properties of the optimal structural configuration, we have used the first-principles density-functional code SIESTA [37,38] to thoroughly relax the final INDIA structures using fully self-consistent calculations. SIESTA employs local basis functions, based on numerical pseudoatomic orbitals, and norm-conserving Troullier-Martins pseudopotentials [39] to solve the Kohn-Sham equations self-consistently within the framework of density functional theory. In this work, we employed double-zeta basis functions and the electronic correlations were handled using the generalized gradient approximation (GGA), via the Perdew-Burke-Ernzerhof (PBE) [40] formulation.

III. RESULTS AND DISCUSSIONS

Since the structural quality of a-Si networks is largely determined by the two- and three-body correlation functions, along with the concentration of dangling and floating bonds (i.e., threefold- and fivefold-coordinated atoms, respectively), we begin by examining the radial and angular correlations between atoms in the models. Noting that the method, by construction, incorporates structural information at the two-body level in real/reciprocal space, we shall focus our attention on network properties that involve higher-order correlation functions, such as the bond-angle distribution (BAD) and dihedral-angle distribution (DAD), statistics of the ring-size distribution, and the local coordinations of atoms in the networks. These will be followed by an analysis of electronic and vibrational properties of the models. Below, we discuss the results from four INDIA models of sizes 216, 300, 512, and 1024 atoms, each averaged over three independent configurations, and provide comparisons with the corresponding WWW and MD models, as well as experimental data from *as-deposited* a-Si samples. For comparison, we generated a set of MD models, using the modified SW potential, following the methodology described in Ref. [30] and refer to those as SW-MD models. Likewise, the WWW models were constructed using the modified bond-switching WWW algorithm of Barkema and Mousseau [18]. In addition, we have also compared our results with a 512-atom model by Deringer *et al.* [23], from using machine-learning-driven MD simulations (ML-MD), 216- and 512-, and 1024-atom models by Pandey *et al.* [13] and Igram *et al.* [16], respectively, from using the force enhanced atomic relaxation (FEAR) approach.

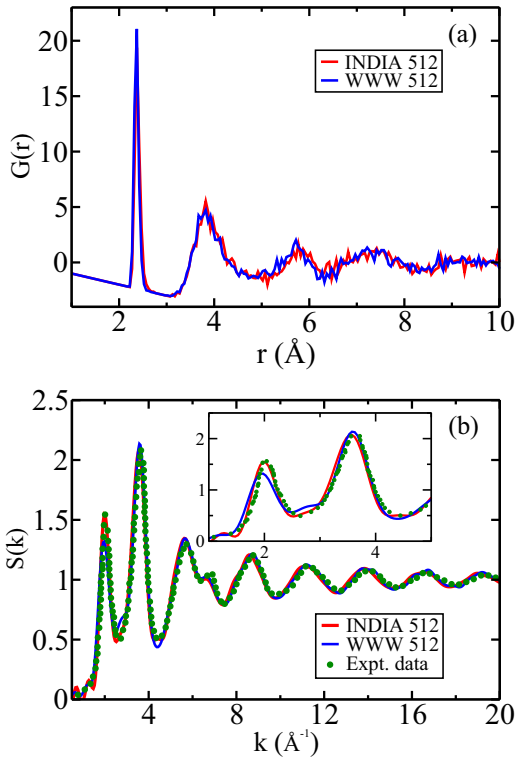

FIG. 3. (a) The reduced pair-correlation functions $G(r)$ of a-Si from INDIA (red) and WWW (blue) models of size 512 atoms. (b) The corresponding static structure factors $S(k)$ from the INDIA (red) and WWW (blue) models. Experimental data for *as-deposited* a-Si samples (green) are included from Ref. [41]. An enlarged view of the first two peaks of the structure factors is shown in the inset for a close comparison of the results.

A. Structural properties

Figure 3 shows the reduced pair-correlation function (PCF) $G(r)$ and the corresponding structure factor (SF) $S(k)$ for the 512-atom INDIA and WWW models. Experimental data from *as-deposited* samples [41] of a-Si are also shown in the plot for comparison. Although the results, in particular the simulated structure-factor data, are expected to match with experiments accurately, it is important to examine the PCF and structure factor closely due to the complementary nature of these (primal and dual) quantities in expressing atomic pair correlations. While a PCF expresses local (two-body) correlations explicitly, its Fourier counterpart provides an overall match (of two-body correlations) incorporating information from all length scales. This is reflected in the first sharp diffraction peaks (FSDP) in Fig. 3(b): the presence of small deviations in $G(r)$ beyond 5.0 Å appears to be translated into

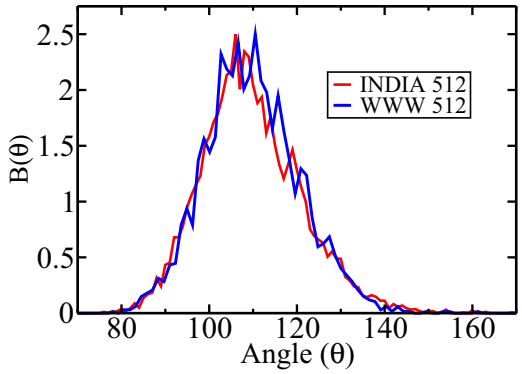

FIG. 4. The bond-angle distributions $B(\theta)$ of a-Si from 512-atom INDIA (red) and WWW (blue) models. The average bond angles and the corresponding root-mean-square deviations are given by $109.1^\circ \pm 11.5^\circ$ (INDIA) and $109.1^\circ \pm 10.7^\circ$ (WWW).

a small but visible difference in the height of the FSDPs [see inset in Fig. 3(b)].

The hierarchy among atomic-correlation functions implies that the one-dimensional PCF/SF alone cannot fully characterize a three-dimensional model of a-Si, unless the PCF/SF is also consistent with, at the very least, the bond-angle distribution (BAD) $B(\theta)$, and its width. Additionally, the latter must be sufficiently narrow so that the network is subjected to minimal structural distortions with a fluctuation in the BAD consistent with the value estimated from Raman spectroscopy [42].These considerations lead to the conclusion that the root-mean-square (RMS) deviation or fluctuation of the bond-angle distribution of a high-quality a-Si network should not exceed 9°–11°. Figure 4 shows the bond-angle distributions for 512-atom INDIA and WWW models. The BADs from the INDIA and WWW models closely match each other, with an average bond angle of $109.1^\circ \pm 10.6^\circ$ (INDIA) and $109.1^\circ \pm 10.5^\circ$ (WWW), obtained from a Gaussian approximation [43] to the shape of the respective BADs. A comparison of structural properties of the models in Table II, obtained from a range of simulation techniques, establishes that the INDIA methodology has the ability to yield a-Si models par excellence. Thus, it would not be inappropriate to conclude that the INDIA models presented here are significantly better than earlier RMC models [1,4] and their hybrid counterparts [12,13,16,44] and that they are on a par with the models obtained from the WWW method and recent high-quality molecular-dynamics simulations [23,30] of amorphous silicon.

Table II summarizes some key structural properties of a-Si models obtained from MD simulations and total-energy-based relaxation methods that are particularly useful for direct comparison. Recognizing that the structural quality of a-Si models is chiefly determined by the PCF, the BAD and its width, and the concentration of coordination defects in the networks and that the FEAR and INDIA methods essentially belong to the same universality class (in the sense that they both rely on the information paradigm), it is evident from Table II that the latter consistently produces a-Si models with a smaller bond-angle width and fewer coordination defects than the FEAR. This observation is indicative of the electronic

TABLE II. Structural properties of *ab initio* relaxed INDIA, MD, and WWW models. $\langle\theta\rangle$, $\Delta\theta(\Delta\theta_G)$, and C_n represent the average bond angles, RMS deviations, and the percentage of n-fold-coordinated atoms, respectively. ΔE is the relative energy difference (in eV) per atom from a 1000-atom crystalline silicon configuration and it is related to heat of crystallization.

Model	N	$\langle\theta\rangle$	$\Delta\theta(\Delta\theta_G)$[a]	C_4	$C_3 + C_5$	ΔE
INDIA	216	109.10	11.8 (11.3)	99.08	0.46 + 0.46	0.232
SW-MD		109.32	8.8 (8.4)	100.0	0.0 + 0.0	0.116
FEAR[b]		108.80	14.6	99.08	0.46 + 0.46	
WWW		109.16	11.1 (10.9)	100.0	0.0 + 0.0	0.185
INDIA	300	109.10	11.4 (10.4)	99.33	0.33 + 0.33	0.219
SW-MD		109.22	9.3 (8.5)	99.33	0.33 + 0.33	0.140
WWW		109.18	10.5 (10.1)	100.0	0.0 + 0.0	0.185
INDIA	512	109.09	11.5 (10.6)	99.60	0.20 + 0.20	0.216
SW-MD		109.27	9.1 (8.6)	99.22	0.39 + 0.39	0.125
ML-MD[c]		109.19	9.7 (9.4)	98.44	0.78 + 0.78	0.138
FEAR[d]				95.90	1.17 + 2.73	
WWW		109.11	10.7 (10.5)	100.0	0.0 + 0.0	0.192
INDIA	1024	109.01	11.9 (10.8)	98.34	1.07 + 0.49	0.236
SW-MD		109.27	8.9 (8.4)	99.22	0.59 + 0.19	0.132
FEAR[d]				94.53	2.34 + 3.13	
WWW		109.14	10.6 (10.3)	100.0	0.0 + 0.0	0.189

[a]Values within parentheses are from a Gaussian approximation.
[b]From Ref. [13].
[c]From Ref. [23].
[d]From Ref. [16].

quality of the models too. We shall see later that, unlike the FEAR models (see Refs. [12,16]), the INDIA models produce a pristine electronic gap around the Fermi level. Further, we shall demonstrate that the size of the electronic gaps obtained from the INDIA models is comparable with those from the WWW models, as far as the models with 216, 300, and 512 atoms are concerned.

In Table II, we have listed the value of $\Delta E = E(N) - E_c$, where $E(N)$ and E_c correspond to the energy per atom for *ab initio* relaxed configurations of a-Si containing N atoms and a crystalline network of silicon comprising 1000 atoms, respectively. The value of E_c has been found to be practically independent of N for $N \geqslant 512$. Here, ΔE is associated with the heat of crystallization of a-Si and has been obtained from differential scanning calorimetry by Roorda *et al.* [45] and Rutherford backscattering and channeling, coupled with differential scanning calorimetry, by Donovan *et al.* [46]. For annealed (at 500 °C) and as-implanted samples of a-Si, the values of ΔE have been determined by Roorda *et al.* to be 13.7 ± 0.7 kJ/mol and 18.8 ± 1.0 kJ/mol, respectively. These values correspond to the range of 0.135–0.205 eV/atom. Likewise, Donovan *et al.* have reported a value of the heat of crystallization to be 11.9 ± 0.7 kJ/mol or 0.116–0.131 eV/atom. Thus, the experimental value of the heat of crystallization matches quite closely with the computed values from the INDIA and SW-MD models.

Probing higher-order correlations between atoms proves to be rather difficult due to the high-dimensional nature of information involving four or more atoms. The distribution of

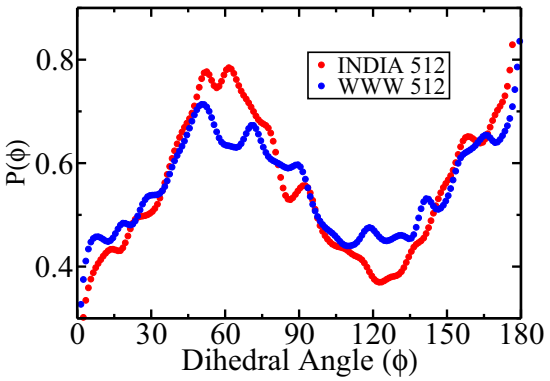

FIG. 5. Dihedral-angle distributions $P(\phi)$ from 512-atom INDIA (red) and WWW (blue) models. The characteristic dihedral peak at 60° and a dip at 120°are distinctly visible in the distributions.

angles between two dihedral planes provides limited information about four-body correlations but it is useful to examine this correlation as an independent check for added credibility. Figure 5 shows the distribution of dihedral angles for two 512-atom INDIA and WWW models. The presence of a characteristic maximum at 60° and a minimum at 120° suggests that the two models are similar as far as the correlations between dihedral angles are concerned. A ball-and-stick representation of a 512-atom INDIA model is shown in Fig. 6.

The connectivity of atoms in amorphous networks can be analyzed by computing the statistics of irreducible rings of varying sizes. Rings are an important feature of topological networks, which are defined as closed irreversible paths or loops that start and end at the same atomic site. Here, irreducibility implies that the ring cannot be further divided into rings of smaller/equal size by topologically deforming the original ring in the space of the embedding dimension. By treating an amorphous network as a *simple connected*

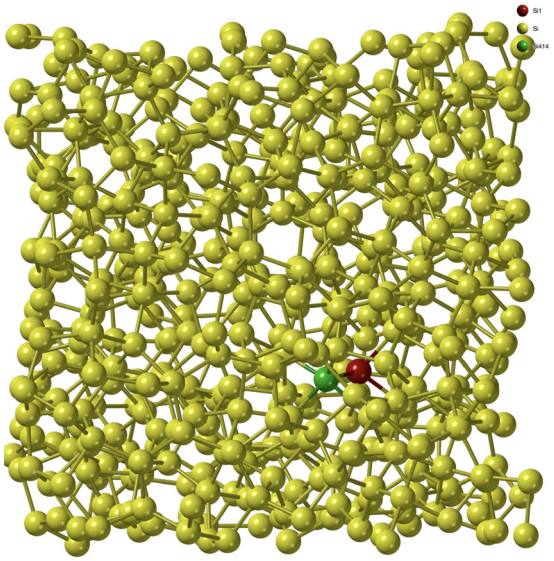

FIG. 6. A ball-and-stick representation of a 512-atom INDIA model with a pair of coordination defects, consisting of a floating (green) bond and a dangling (red) bond. The remaining fourfold-coordinated Si atoms are shown in yellow color.

TABLE III. Ring statistics for INDIA, WWW, and two MD models comprising $N = 216, 300, 512, 1024$ atoms. Columns 3 to 8 list the number of rings per atom from ring sizes 4 to 9, respectively.

Model	N	4	5	6	7	8	9
INDIA	216	0.005	0.389	0.889	0.611	0.139	0.032
SW-MD		0	0.278	1.125	0.676	0.060	0.009
WWW		0.028	0.444	0.745	0.528	0.171	0.040
INDIA	300	0.017	0.403	0.860	0.537	0.173	0.023
SW-MD		0.007	0.353	0.990	0.597	0.107	0.017
WWW		0.003	0.420	0.857	0.537	0.133	0.020
INDIA	512	0.018	0.404	0.789	0.613	0.152	0.014
SW-MD		0.008	0.359	0.939	0.619	0.133	0.023
ML-MD[a]		0.014	0.389	0.856	0.643	0.104	0.018
WWW		0.039	0.467	0.717	0.465	0.191	0.033
INDIA	1024	0.020	0.422	0.785	0.535	0.157	0.035
SW-MD		0.003	0.320	1.044	0.609	0.094	0.021
WWW		0.026	0.443	0.754	0.505	0.153	0.027

[a]From Ref. [23].

graph $G = (V, E)$, where $V(G)$ is a vertex set consisting of atomic centers and $E(G)$ is an edge set consisting of bonds between two nearest-neighbor atoms, one can obtain the irreducible ring-size distribution by computing the adjacency matrix of $V(G)$. Table III lists the irreducible-ring statistics for a number of INDIA, WWW, and two MD models, obtained using periodic boundary conditions. The results for these four 512-atom models are presented in Fig. 7. It is apparent that the ring-size distributions in the INDIA and WWW models are essentially similar, whereas the SW-MD model shows a comparatively high number of six-member rings in the network. Table III confirms that this observation also applies to the rest of the SW-MD models. A comparison with the results obtained from 216-, 300-, and 1024-atom INDIA and WWW models leads us to believe that this *excess topological crystal-like feature* of SW-MD models could be attributed to the modified SW potential, which exhibits a tendency to form diamond crystals during MD simulations. It is also plausible that MD simulations can sample the solution space more accurately than a total-energy-based relaxation method

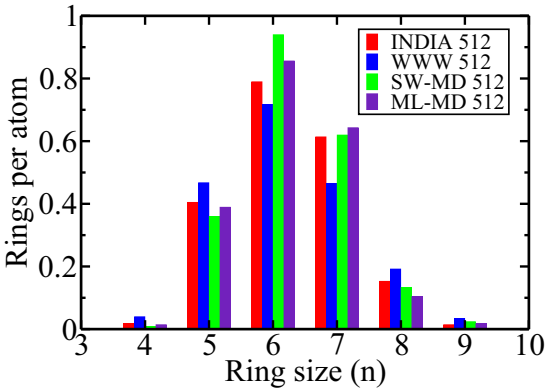

FIG. 7. Ring statistics for four different models of a-Si of size 512 atoms. The SW-MD model shows a relatively strong presence of six-member rings compared to its WWW and INDIA counterparts.

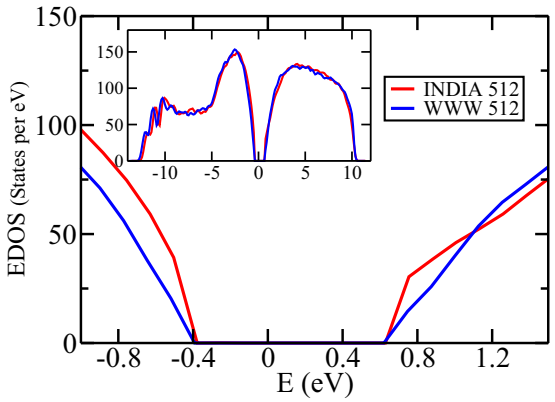

FIG. 8. The densities of electronic states of *a*-Si from INDIA (red) and WWW (blue) models with the Fermi level at 0.0 eV. A pristine electronic gap of size approximately 1 eV is clearly visible.

in determining a low-energy structure, which is topologically closer to the crystalline diamond network. The values of ΔE for the MD models, listed in Table II, appear to support this conjecture. In the future, we expect to address this issue by taking into account the presence of a few coordination defects that may affect the ring-size distribution.

B. Electronic and vibrational properties

While the results in the preceding section establish the structural quality of the INDIA models, a strong coupling between local environments of atoms and the vibrational and electronic degrees of freedom in *a*-Si warrants further examination to validate the vibrational and electronic properties of the models. A good atomistic model of *a*-Si must exhibit a clean electronic band gap around the Fermi level and the size of the gap should determine the electronic quality of the model, by jointly taking into account the structural quality and the density of coordination defects in the network. Although theoretical considerations [47] lead to the existence of such a spectral gap in tetrahedral amorphous networks, it has been noted that the size of the gap and the density of states in its vicinity are particularly susceptible to coordination defects. Until the recent developments of high-quality MD models [23,30], only WWW models were capable of producing a clean gap in the electronic spectrum around the Fermi level. It is therefore imperative to validate the accuracy of new atomistic models by computing the EDOS and the size of the gap therefrom. Likewise, the energy required to excite vibrational degrees of freedom in *a*-Si, typically a few tens of meV, suggests that the latter can be very sensitive to local atomic arrangements, which may not be apparent in the electronic spectrum. Thus, a final analysis should also include a statement on the vibrational density of states of the models.

Figure 8 depicts the EDOS for 512-atom INDIA and WWW models, with the Fermi levels at 0 eV. The INDIA model produces a clean gap, which accurately matches the same from the WWW model. This observation also applies to the 216- and 300-atom INDIA models. Table IV lists the values of the band gaps obtained from four INDIA models, along with the corresponding values from the WWW and SW-MD models. The results can be summarized by making

TABLE IV. Comparison of band-gap values (in eV) for *a*-Si models obtained from the INDIA, WWW, and SW-MD simulations.

Model size	216	300	512	1024
INDIA	0.753	0.884	1.007	0.38
WWW	1.007	1.008	1.013	1.012
SW-MD	1.003	0.881	1.006	1.009
Experiments[a]		1.6–1.75		

[a]Quoted values are for device-grade *a*-Si:H from Ref. [49].

the following observations: (1) The EDOS and the size of the gap from the 512-atom INDIA model match accurately with the corresponding results from the WWW and SW-MD models (cf. Table IV). (2) A small but noticeable difference in the shape of the valence-band tails for the 512-atom INDIA and WWW models in Fig. 8 can be attributed to a combination of the lack of statistics and the different degree of disorder associated with bond angles and bond lengths, and ΔE of the networks (0.22 eV for INDIA vs 0.19 eV for WWW). (3) A small value of the band gap (0.38 eV) noted for the 1024-atom INDIA model points to the presence of 1.6% coordination defects and, possibly, the presence of a few strained bonds, as indicated by a slightly higher value of $\Delta E = 0.24$ eV. Overall, the electronic properties of the INDIA models are on a par with the WWW models.

Finally, Fig. 9 shows the vibrational densities of states of 512-atom INDIA and WWW models, obtained by diagonalizing dynamical matrices that were constructed in the harmonic approximation, along with the experimental data from inelastic neutron-scattering measurements by Kamitakahara *et al.* [48]. The computed VDOS from the INDIA model agrees well with experiments. In particular, the VDOS from the INDIA model in the region from 300 cm^{-1} to 600 cm^{-1} has been found to fit more accurately with experimental data than its WWW counterpart.

IV. CONCLUSIONS

In this work, we have presented an information-driven inverse approach, or INDIA, to invert experimental diffraction

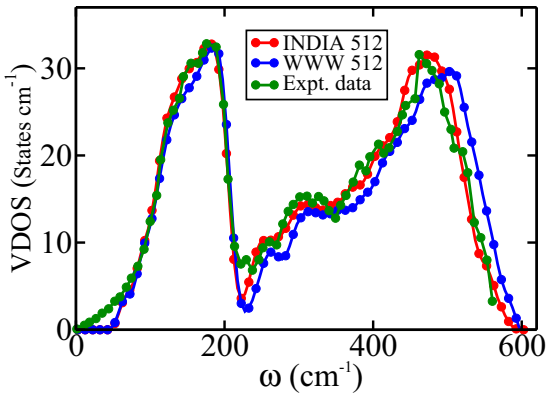

FIG. 9. The vibrational densities of states (VDOS) of *a*-Si from 512-atom INDIA (red) and WWW (blue) models. Experimental data from inelastic neutron-scattering measurements, from Ref. [48], are also shown for comparison.

data in conjunction with a few structural constraints and a total-energy functional. Since one-dimensional scattering data alone cannot describe a three-dimensional distribution of atoms uniquely, and the presence of too many structural constraints can make the inversion problem somewhat ill posed, we have followed a hybrid strategy to augment the dimension of the search space in an effort to determine an accurate structural solution of the inversion problem, aided by a total-energy functional. It has been shown that the original inversion problem can be posed as a nonconvex optimization problem in an extended or augmented search space that involves information from a set of experimental diffraction data, a few structural constraints, and an approximate total-energy functional of the system. We then demonstrate that the complexity associated with solving the resulting optimization program can be considerably reduced by decomposing the extended objective function into two subspace objective functions and optimizing these two functions sequentially in a self-consistent way.

An examination of the optimal structural models, consisting of up to 1024 atoms, shows that the vibrational, electronic, and structural properties of the models match accurately with the corresponding experimental data from *as-deposited* samples of amorphous silicon. In particular, the first sharp diffraction peak of a 512-atom INDIA model has been found to match somewhat more accurately with experimental structure-factor data than its corresponding WWW counterpart. Likewise, a comparison of the vibrational density of states (VDOS) with inelastic neutron-scattering data reveals that the 512-atom INDIA model reproduces the density of high-frequency vibrations more accurately than the corresponding WWW model. Further analyses of various structural properties, involving the pair-correlation function, the bond- and dihedral-angle distributions, and the statistics of n-member irreducible rings ($n = 4$ to 9) in the networks, show that the INDIA models are on a par with the high-quality WWW models and those obtained from recent high-quality MD simulations using the modified Stillinger-Weber and machine-learning-driven potentials. The electronic densities of states, specifically the ones from 300- and 512-atom models, obtained from a local-basis density-functional code SIESTA using the generalized gradient approximation, show the presence of a pristine gap in the electronic spectrum in the vicinity of the Fermi level, with only a pair of coordination defects. The size of the electronic gaps from the INDIA models is found to be comparable with those from the corresponding WWW models. Furthermore, the estimated values of the heat of crystallization of the models closely compare with those obtained by Roorda *et al.* [45] and Donovan *et al.* [46] from differential scanning calorimetry measurements. In conclusion, the information-driven approach and its implementation presented here can successfully invert a set of diffraction data and structural constraints in conjunction with a total-energy functional by producing atomistic models of *a*-Si, which are significantly better than existing hybrid RMC models of *a*-Si and are on a par with the WWW models, as far as the structural, electronic, and vibrational properties of *a*-Si are concerned.

ACKNOWLEDGMENTS

The work was partially supported by the U. S. National Science Foundation (NSF) under Grants No. DMR 1507166, No. DMR 1507118, and No. DMR 1506836. The authors thank N. Mousseau (Montreal, Canada) and G. Barkema (Utrecht, The Netherlands) for providing their modified WWW code. We acknowledge the use of computing resources at the University of Southern Mississippi, supported by the NSF under the Major Research Instrumentation (MRI) program via Grant No. ACI 1626217. The authors thank the anonymous referees for suggesting Ref. [46] and a few subtle changes associated with the notation in the text.

[1] P. Biswas, R. Atta-Fynn, and D. A. Drabold, Phys. Rev. B **69**, 195207 (2004).
[2] J. K. Walters and R. J. Newport, Phys. Rev. B **53**, 2405 (1996).
[3] R. L. McGreevy, J. Phys.: Condens. Matter **13**, R877 (2001).
[4] O. Gereben and L. Pusztai, Phys. Rev. B **50**, 14136 (1994).
[5] M. G. Tucker, D. A. Keen, M. T. Dove, A. L. Goodwin, and Q. Hui, J. Phys.: Condens. Matter **19**, 335218 (2007).
[6] M. H. Brodsky and R. S. Title, Phys. Rev. Lett. **23**, 581 (1969).
[7] A. Kirsch, *An Introduction to the Mathematical Theory of Inverse Problems* (Springer, New York, 1996).
[8] M. Born and H. S. Green, Proc. R. Soc. London A **188**, 10 (1946).
[9] J. G. Kirkwood, J. Chem. Phys. **14**, 180 (1946).
[10] P. Biswas, D. N. Tafen, and D. A. Drabold, Phys. Rev. B **71**, 054204 (2005).
[11] P. Biswas, R. Atta-Fynn, and D. A. Drabold, Phys. Rev. B **76**, 125210 (2007).
[12] A. Pandey, P. Biswas, and D. A. Drabold, Phys. Rev. B **92**, 155205 (2015).
[13] A. Pandey, P. Biswas, and D. A. Drabold, Sci. Rep. **6**, 33731 (2016).
[14] M. J. Cliffe, M. T. Dove, D. A. Drabold, and A. L. Goodwin, Phys. Rev. Lett. **104**, 125501 (2010).
[15] M. J. Cliffe, A. P. Bartók, R. N. Kerber, C. P. Grey, G. Csányi, and A. L. Goodwin, Phys. Rev. B **95**, 224108 (2017).
[16] D. Igram, B. Bhattarai, P. Biswas, and D. Drabold, J. Non-Cryst. Solids **492**, 27 (2018).
[17] F. Wooten, K. Winer, and D. Weaire, Phys. Rev. Lett. **54**, 1392 (1985).
[18] G. T. Barkema and N. Mousseau, Phys. Rev. B **62**, 4985 (2000).
[19] B. R. Djordjević, M. F. Thorpe, and F. Wooten, Phys. Rev. B **52**, 5685 (1995).
[20] B. Meredig and C. Wolverton, Nat. Mater. **12**, 123 (2013).
[21] P. Biswas, D. N. Tafen, R. Atta-Fynn, and D. Drabold, J. Phys.: Condens. Matter **16**, S5173 (2004).
[22] P. Biswas, R. Atta-Fynn, S. Chakraborty, and D. A. Drabold, J. Phys.: Condens. Matter **19**, 455202 (2007).
[23] V. L. Deringer, N. Bernstein, A. P. Bartók, M. J. Cliffe, R. N. Kerber, L. E. Marbella, C. P. Grey, S. R. Elliott, and G. Csányi, J. Phys. Chem. Lett. **9**, 2879 (2018).
[24] P. Biswas, D. A. Drabold, and R. Atta-Fynn, J. Appl. Phys. **116**, 244305 (2014).

[25] P. Biswas and R. Timilsina, J. Phys.: Condens. Matter **23**, 065801 (2011).
[26] R. Timilsina and P. Biswas, J. Phys.: Condens. Matter **25**, 165801 (2013).
[27] P. Biswas, D. Paudel, R. Atta-Fynn, D. A. Drabold, and S. R. Elliott, Phys. Rev. Appl. **7**, 024013 (2017).
[28] K. Prasai, P. Biswas, and D. A. Drabold, Sci. Rep. **5**, 15522 (2015).
[29] P. Biswas and S. R. Elliott, J. Phys.: Condens. Matter **27**, 435201 (2015).
[30] R. Atta-Fynn and P. Biswas, J. Chem. Phys. **148**, 204503 (2018).
[31] J. Hadamard, *Lectures on the Cauchy Problem in Linear Partial Differential Equations* (Yale University Press, New Haven, 1923).
[32] The phrase "well posed" is used here in a Hadamard sense. Following Hadamard [31], a problem is well posed if a mathematical model of the physical problem has the properties of uniqueness, existence, and stability of the solution. In the present context, assuming that the first two properties are satisfied in the presence of structural constraints, it is not evident that the solution [of Eq. (1)] continuously depends upon experimental data and constraint information. By including additional *a priori* information, it is often possible to augment the solution space and improve the smoothness and stability of the solution with respect to input data. This study is a case in point.
[33] Here, we are optimizing the values of χ_M and χ_K by varying $\mathbf{R}$, and $\mathcal{M}$ and $\mathcal{K}$ denote the set of all possible values χ_M and χ_K, respectively, obtained via the mapping $f : \mathbf{R} \rightarrow \chi$. The map f is defined by Eq. (2) and the objective functions χ_M and χ_K are two-dimensional vectors or 2-tuple objects in the subspaces $\mathcal{M}$ and $\mathcal{K}$, respectively.
[34] The constraint function $C_l(\mathbf{R})$ corresponds to the square of the deviation of the average coordination $n_l(\mathbf{R})$ from an ideal target value of n_0. Here, we have used the following functional form of $C_l(\mathbf{R})$:

$$C_l(\mathbf{R}) = \sum_l \left(1 - \frac{n_l(\mathbf{R})}{n_0}\right)^2.$$

A value of $\lambda_l = 1$ to 5 and $n_0 = 4$ have been observed to work well in our work.
[35] R. Vink, G. Barkema, W. van der Weg, and N. Mousseau, J. Non-Cryst. Solids **282**, 248 (2001).
[36] F. H. Stillinger and T. A. Weber, Phys. Rev. B **31**, 5262 (1985).
[37] J. M. Soler, E. Artacho, J. D. Gale, A. García, J. Junquera, P. Ordejón, and D. Sánchez-Portal, J. Phys.: Condens. Matter **14**, 2745 (2002).
[38] E. Artacho, D. Sánchez-Portal, P. Ordejón, A. García, and J. M. Soler, Phys. Status Solidi B **215**, 809 (1999).
[39] N. Troullier and J. L. Martins, Phys. Rev. B **43**, 1993 (1991).
[40] J. P. Perdew, K. Burke, and M. Ernzerhof, Phys. Rev. Lett. **77**, 3865 (1996).
[41] K. Laaziri, S. Kycia, S. Roorda, M. Chicoine, J. L. Robertson, J. Wang, and S. C. Moss, Phys. Rev. B **60**, 13520 (1999).
[42] D. Beeman, R. Tsu, and M. F. Thorpe, Phys. Rev. B **32**, 874 (1985).
[43] The application of a Gaussian approximation to the shape of the bond-angle distribution (BAD) somewhat underestimates the width of the BAD. Since a Gaussian distribution is uniquely defined by the first two moments of the distribution, and these two moments cannot determine the tail structures of a distribution accurately (without the knowledge of higher moments), the presence of a few large/small angles in a bond-angle distribution cannot be taken into account in the calculation of its width using a Gaussian approximation. The results presented in Table II are consistent with this observation.
[44] A. Pandey, P. Biswas, B. Bhattarai, and D. A. Drabold, Phys. Rev. B **94**, 235208 (2016).
[45] S. Roorda, W. C. Sinke, J. M. Poate, D. C. Jacobson, S. Dierker, B. S. Dennis, D. J. Eaglesham, F. Spaepen, and P. Fuoss, Phys. Rev. B **44**, 3702 (1991).
[46] E. P. Donovan, F. Spaepen, D. Turnbull, J. M. Poate, and D. C. Jacobson, Appl. Phys. Lett. **42**, 698 (1983). .
[47] D. Weaire and M. F. Thorpe, Phys. Rev. B **4**, 2508 (1971).
[48] W. A. Kamitakahara, H. R. Shanks, J. F. McClelland, U. Buchenau, F. Gompf, and L. Pintschovius, Phys. Rev. Lett. **52**, 644 (1984).
[49] S. Kageyama, M. Akagawa, and H. Fujiwara, Phys. Rev. B **83**, 195205 (2011).